[1] Acousto-optical full-field stereoscopic spectrometer for 3d reconstruction in an arbitrary spectral interval

A.S. Machikhin[1,2], V.I. Batshev[1,3] , V.E. Pozhar[1,4] , M.M. Mazur[1,5]
[1] Scientific and Technological Center of Unique Instrumentation of the Russian Academy of Sciences, Moscow, Russia
[2] National Research University "MPEI", Moscow, Russia
[3] Bauman Moscow State Technical University, Moscow, Russia
[4] National Research Nuclear University "MEPhI", Moscow, Russia
[5] All-Russian Scientific Research Institute of Physical-Technical and Radioengineering Measurements (VNIIFTRI), Mendeleyevo, Moscow Region, Russia

Abstract

A problem of spectral narrowband 3D imaging in the visible spectral range is considered. A double-channel acousto-optical spectral system is developed to acquire stereoscopic images in cross-polarized optical beams. A prototype is presented. Some examples of stereoimages detected with the instrument are presented and a 3D image reconstructed on their basis is described.

Keywords: *spectroscopy, acoustooptic, 3D imaging.*

Citation: *Machikhin AS, Batshev VI, Pozhar VE, Mazur MM. Acousto-optical full-field stereoscopic spectrometer for 3D reconstruction in an arbitrary spectral interval. Computer Optics 2016; 40(6): 871-877. DOI: 10.18287/2412-6179-2016-40-6-871-877.*

Introduction

Devices intended for visualization and analysis of two-dimensional object structures in individual spectral intervals are now widely used in researches [1,2]. Spectral filtration allows a system to operate with images particularly in those wavelength intervals where there are no background noises, and physical, chemical, and other properties of analyzed objects are exerted more intensively. For this purpose, the light is accentuated in absorption, emission or fluorescence bands of visualized materials. Besides, there are many industrial, medical, biological, and other problems where spatial property distribution for objects with contoured (three-dimensional), not flat, surfaces must be investigated. So, basically, it is necessary to obtain more information on the arrangement and the shape of elements of a prototype [3,4].

Additional information in respect to one particular coordinate – spatial (z) or spectral (λ), being added to the classical 2D image $I(x,y)$ recording system, provides completely new quality of object imaging: stereoscopic imaging $I(x,y,z)$ or spectral visualization $I(x,y,\lambda)$ [5]. These two coordinates instantly added thereto would facilitate obtaining even better analytical effect, i.e. registering four-dimensional distributions $I(x,y,z,\lambda)$. For example, many microscopes intended for stereoscopic recording are supplied with several spectral filters provided for object contrast enhancement. However, this allows us to acquire 3D images only within a few fixed spectral bands. There have been no devices generating 3D images at arbitrary wavelengths λ as yet. Therefore, the problem of development of such devices is deemed to be of current interest.

This paper describes an acousto-optic stereoscopic imaging spectrometer operating on the principle of simultaneous spectral filtration of two light beams that transfer images of an object observed from two different perspectives through one input lens as compared to the layout of an Abbe stereoscopic microscope [6]. A distinguishing feature of the developed device is the varying polarization for two images that form a stereo pair. It provides some additional information that is important for solving various biomedical problems.

1. Operation principle

Radiation must be additionally passed through an optical filter in order to receive spectral imaging. A set of interchangeable optical light filters or a tunable optical filter may be used for this purpose. Acousto-optic filters which have no moving elements are best suited for this purpose. They provide fast arbitrary spectral addressing, a high transmission factor, and rather high spatial and spectral resolution [7,8].

Transferring images requires a large angular aperture attained in wide-angularacousto-optic filters [9]. A formal condition for implementing wide-angulardiffraction geometry in the *ZX*-plane of a uniaxial crystal containing an optic axis of the *Z* crystal is the parallelism of tangent lines in wave-vector space compared to wave surfaces for incident and diffracted waves (Fig. 1a). For this purpose, angles of propagation of incident θ and diffracted ψ light waves for diffraction cases $o \rightarrow e$ and $e \rightarrow o$ must be bound by the following equations [9]:

$$\begin{aligned} \Psi_e &= arcctg\left(\left(1/\xi_0^2\right)ctg\theta_o\right), \\ \Psi_o &= arcctg\left(\xi_0^2 ctg\theta_e\right), \end{aligned} \qquad (1)$$

where $\xi_0 = n_e/n_o$ is the birefringence parameter. In these cases, the angle of acoustic wave propagation γ is as follows [9,10]:

$$\begin{aligned} \gamma_{oe} &= arctg\left(\frac{ctg\,\theta_o}{\sqrt{\left(ctg^2\theta_o+1\right)\left(ctg^2\theta_o+\xi_0^2\right)}+ctg^2\theta_o}\right), \\ \gamma_{eo} &= arctg\left(\frac{\hat{\imath}\;ctg\,\theta_e}{\xi^3\,ctg^2\theta_e+\sqrt{\left(\xi^4\,ctg^2\theta_e+1\right)\left(\xi^2\,ctg^2\theta_e+1\right)}}\right). \end{aligned} \qquad (2)$$

The interaction of the light θ and sound γ orientation angles in the wide-angular diffraction denoted by the above formulas (2) take the form of nonmonotone curves; therefore, the direction of sound propagation γ may be the same for two different polarizations. This allows us to use two identical acousto-optic cells wherein the light is to be beamed at the angles θ_o and θ_e. Figure 1b shows a configuration of such a cell as exemplified by diffraction of the o-polarized light. The second cell is fully identical thereto and is flipped in the XZ-plane through 180° in such a way that the light comes in as the e-polarized and comes out as the o-polarized light. Thus we can also analyze the state of radiation polarization moving away from the object.

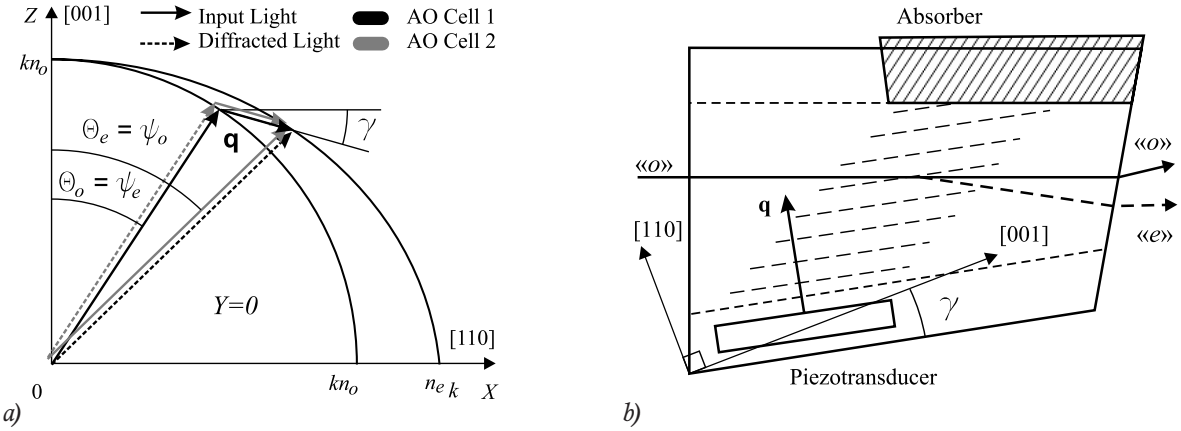

Fig. 1. Wave-vector diagram (a) and architecture (b) of acous-to-optical cells

Two acousto-optical cells have been made of optically anisotropic crystal TeO_2. They have the same identical wide-angular geometry with the angle of sound propagation $\gamma = 6°$. Its wave-vector diagram is shown in Fig. 1a. The symbol **q** denotes a sound vector which is directed at the angle 6° to the *OX* axis. For this purpose, the *o*-polarized radiation is entered into the first acousto-optic cell at the angle $\theta_o = 12.2°$ and it comes out as the extremely *e*-polarized radiation at the angle $\theta_e = 13.8°$, whereas in the second cell it's quite the opposite. A longitudinal acoustic wave is generated in the acousto-optical cell, which, after being reflected from the crystal edge, is transferred into a transverse wave whereon the light is subsequently diffracted [11,12].

A double-channel monochromator based on such acousto-optical cells has the following characteristics: the tuning range is 440-760 nm, the spectral resolution is $\delta\lambda = 2.5$ nm (at the wavelength $\lambda = 633$ nm), the control ultrasonic frequency range is 65-127 MHz, the length of a piezoelectric transducer is 9 mm, the angular field of view is 3°×3°, the entrance pupils are in the shape of vertically extracted rectangles 6×8 mm² in size. A stereo imaging principle is as follows. A prototype object is placed in the front focal plane of the optical system directing collimated beams into two channels of the acousto-optical monochromator. Two monochromatized, orthogonally polarized light beams are focused on certain radiation detectors. Two recorded images forming a stereoscopic pair are later processed using the computer vision method.

2. Pilot plant

The optical beam path in the acousto-optical stereoscopic spectrometer and its control diagram are given in Fig. 2a. Lens 2 is forming a pair of light beams, which transfer the image of Object 1 in two different perspectives and directs it onto the entrance of the double-channel acousto-optical monochromator. The monochromator contains two identical Acousto-Optical Cells 4 and 7 flipped through 180° and two pairs of Crossed Polarizers 3, 5 and 6, 8. A spectral light component satisfying a Bragg condition (Fig. 1a) diffracts on acoustic beams in both acousto-optical cells with changing linear polarization for orthogonal polarization ($o \to e$ and $e \to o$) and small deviation.

Nondiffracted radiation is delayed by Exit Polarizers 5 and 8. After having passed the acousto-optical monochromator, two orthogonally polarized beams carrying stereoscopic object images are deviated by two different edges of Mirror Prism 9 and are focused by Lenses 10 and 12 on Photodetector Arrays 11 and 13. A pair of recorded images is processed with the aid of Computer 18. The computer also provides the total system control assigning a proper mode of operation and parameters of the acousto-optical monochromator and Detectors 11 and 13. The wavelength of radiation λ evolved by the acousto-optical filters in both channels is defined by the frequency *f* of high-frequency (HF) signals generated by Generator 15 and amplified by a pair of High-Frequency Amplifiers 16 and 17. A general layout of the stereoscopic spectrometer (without control unit and computer) is given in Fig. 2b.

The computation as described below was performed to determine optical characteristics of the system. It should be noted that since all optical characteristics of the element are the same in both channels of the acousto-optical stereoscopic spectrometer, the computation of one channel would be generally true for another one.

The initial computation parameters are as follows: the total field angle of each channel 2ω having comprised 3° on both directions, as well as the size of an entrance pupil and dimensions of the detector and a certain pixel. Taking into consideration the fact that entrance pupils of the acousto-optic monochromator have the form of rectangles 6×8 mm² in size, the pupil was considered to be round-shaped with diameter $D = 8$ mm in further computations. The CMOS image sensors *Aptina MT9V024* with 6×6 μm² size pixel and 744×480 number of pixels were used in the capacity of detector arrays which is equivalent to the array size 4.8×3.6 mm² (1/3″ diagonal). Exit Lens 10 with the focal length $f_{10} = 50$ mm ensures the field of view 5.5°×4° which exceeds the field of view of the acousto-optical monochromator and ensures any radiation having passed therethrough to be captured.

Entrance Lens 2 is made changeable thus to allow us to form an image with differential linear optical magnification as follows:

$$\beta = f_{10} / f_2 , \qquad (3)$$

where f_2 is the focal length of Entrance Lens 2. Though a standard photolens may be used for this purpose, a special-purpose high-performance lens was applied to ensure the best imaging quality. To block apertures of both channels of the acousto-optical monochromator, its diameters had to be 20°mm. The linear field of the spectrometer equaled to the largest size of the imaged object is as follows:

$$2y = 2 f_2 \operatorname{tg} \omega . \qquad (4)$$

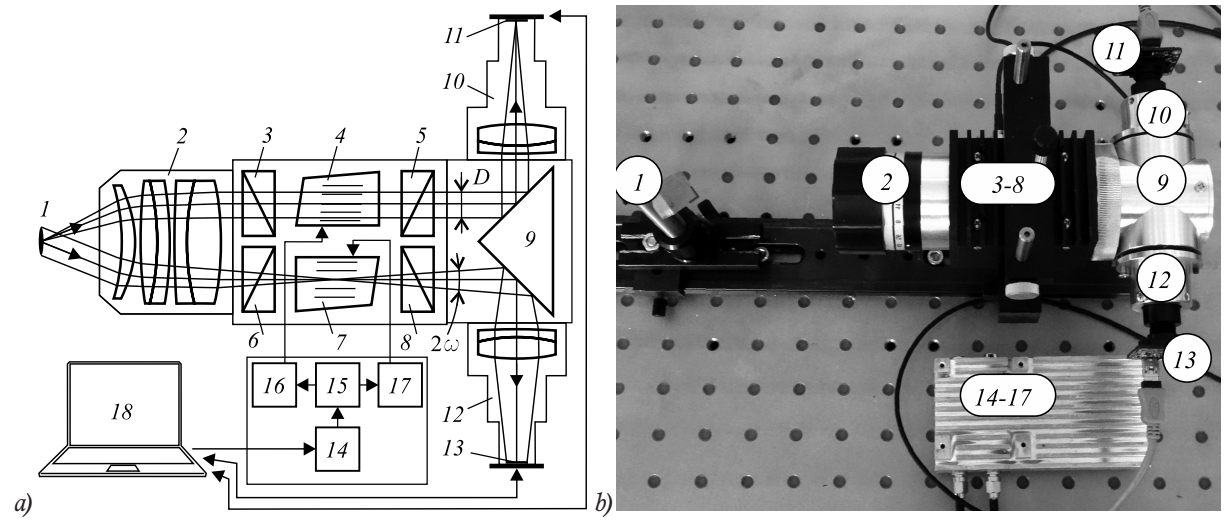

Fig. 2. Layout of the spectrometer (a) and external view of a prototype (b): 1 – observed object, 2 – entrance lens, 3, 5, 6, 8 – polarizers, 4, 7 – acousto-optical cells, 9 – mirror prism, 10, 12 – lenses, 11, 13 – detector arrays, 14 – controller, 15 – HF generator, 16, 17 – HF amplifiers, 18 – computer. Radiation is equally distributed through both channels. For illustrative purposes, only an on-axial beam is shown in the upper channel, whereas main beams radiating from various points of the object are shown in the bottom channel. Beam deflection during diffraction in the acousto-optical cells is not shown either

The most important parameter of the stereoscopic optical system is the depth of roughly imaged space which can be estimated from the following considerations [6]. Displacement of the object along the optical axis by a value of z results in displacement of its image by the following value:

$$z' = \alpha \cdot z , \quad (5)$$

where α is the longitudinal magnification of the spectrometer optical system equaled to $\acute{a} = \hat{a}^2$. This accordingly results in blurring a point image as follows:

$$\delta' = z' D / f_{10} , \quad (6)$$

and restrains a resolution limit in the subject space as follows:

$$\delta = \delta' / \beta . \quad (7)$$

Thus the depth of roughly imaged space is determined by a maximum allowed value of the resolution limit δ and the focal length of the entrance lens f_2 as follows:

$$z = \delta \cdot f_2 / D . \quad (8)$$

The influence of chromatic aberrations of the acousto-optical filter has not been considered in the above formulas. However, its spectral bandpass is rather narrow (2.5 μm) thus providing for a good spatial resolution of the device [13].

The entrance lens with the focal length f_2 = 50 mm has been used in the prototype. That provides the following characteristics: the linear magnification β = 0.5, the field of view $2y$ = 2.6 mm, and the depth of sharply imaged space z = ±0.6 mm (when the allowable resolution limit is δ = 0.1 mm).

3. Data measurement and processing

A cube 4.5 mm in size was used as a test object for the stereoscopic spectrometer. Its surface contains various colorful square sections. The comparison of spectral images on two different wavelengths λ_1 = 600 nm and λ_2 = 750 nm (Fig. 3a) shows that during spectrum agility the borderlines between different sections are contrasted with the image. Spectral characteristics of all image points can be built using the measurement series with the minimum spectrum pitch $\delta\lambda$ followed by exact registration of spectral snapshots in case of preliminary calibration of the system spectral sensitivity. To obtain 3D spectral images it is necessary to perform the following procedures as described below.

Preliminary space calibration of the spectrometer is required to reconstruct, by image pairs, a surface shape of the test object and to build its 3D model in the form of point sets forming its surface in order to determine characteristics for each channel and parameters of mutual channel orientation [14-16].

The calibration matrix **C** used in measurement processing is determined in terms of the series of 3D test object images on the surface of which some special marks have been applied. Their local coordinates ($\mathbf{M} \equiv (X,Y,Z)^T$) in the object-related coordinate system are counted with high precision. A steel cube 15 mm in size was used in the quality of such test object. A hatch grid, 50 μm in

width and 0.2 mm in spacing, has been gridded at cube faces in the neighborhood of a spectrometer-faced top using the laser engraving technique. Determining the coordinates (u,v) of grid nodes on the recorded images, we can calculate a 3x3 matrix $\mathbf{A_1}$ of inherent characteristics of the first channel and parameters **(R', t')** thereof that characterize its orientation with respect to its global object-related coordinate system using the following set of equations [17]

$$Z'\mathbf{v}' = \mathbf{A}_1\mathbf{R}'\mathbf{M} + \mathbf{t}' = \mathbf{C}_1\tilde{\mathbf{M}}, \quad (9)$$

where $\mathbf{v}' = (u,v,1)^T$ is the coordinate vector on the image in the first channel, Z' is a certain object distance, **t'** and **R'** is a vector distance and a rotation matrix describing transition from the object-related global coordinate system to the coordinate system of the first channel $\tilde{\mathbf{M}}=(X,Y,Z,1)$.

Components of the identified matrix $\mathbf{A_1}$ are defined by pixel sizes in the photoelectric detector, the position of the principal point, and the focal distance of the first channel optics. Similarly determining a calibration matrix $\mathbf{C_2}$ of the second channel and its inherent parameters $\mathbf{t}'$ and $\mathbf{R}'$, we can define parameters of mutual channel arrangement: $\mathbf{R} = \mathbf{R''R}'^{\mathrm{T}}$, $\mathbf{t} = -\mathbf{R''R}'^{\mathrm{T}}\mathbf{t}' + \mathbf{t''}$ that completely accomplishes calibration of a stereo system.

While measuring and rebuilding the object (in manual or automatic modes), there are some conjugate points in two pictures. Their coordinates **v'** and **v**′ are determined. Once this is done the object distance of two spectrometer channels Z', Z'' can be easily calculated as follows [17]:

$$\begin{bmatrix} Z' \\ Z'' \end{bmatrix} = \begin{bmatrix} \mathbf{v}'^{\mathrm{T}}\mathbf{A}_1^{-\mathrm{T}}\mathbf{A}_1^{-1}\mathbf{v}' & -\mathbf{v}'^{\mathrm{T}}\mathbf{A}_1^{-\mathrm{T}}\mathbf{R}^{\mathrm{T}}\mathbf{A}_2^{-1}\mathbf{v}'' \\ -\mathbf{v}'^{\mathrm{T}}\mathbf{A}_1^{-\mathrm{T}}\mathbf{R}^{\mathrm{T}}\mathbf{A}_2^{-1}\mathbf{v}'' & \mathbf{v}''^{\mathrm{T}}\mathbf{A}_2^{-\mathrm{T}}\mathbf{A}_2^{-1}\mathbf{v}'' \end{bmatrix} \cdot \begin{bmatrix} -\mathbf{v}'^{\mathrm{T}}\mathbf{A}_1^{-\mathrm{T}}\mathbf{R}^{\mathrm{T}} \\ -\mathbf{v}''^{\mathrm{T}}\mathbf{A}_2^{-\mathrm{T}} \end{bmatrix} \mathbf{t}. \quad (10)$$

Then, using the following formulas,

$$\begin{aligned} Z'\mathbf{v}' &= \mathbf{A}_1\mathbf{M}' \\ Z''\mathbf{v}'' &= \mathbf{A}_2\mathbf{M}'' \end{aligned} \quad (11)$$

we can determine the 3D coordinates **M'** and **M**″ of the selected point within the coordinate system for two channels.

Figure 3a shows the examples of 10 pairs selected in stereoscopic images (**v'** and **v''**) of conjugate points. Figure 3b gives the computing result of the above method for the 3D coordinates (X,Y,Z) of relevant points in the coordinate system where zero is coincided with the point *O*. It can be seen that obtained values are close to true values and restored contours follow the actual shape of the test object.

A three-dimensional structure of the object surface can be similarly determined on photos in any spectral interval within a tuning range of the acousto-optical monochromator.

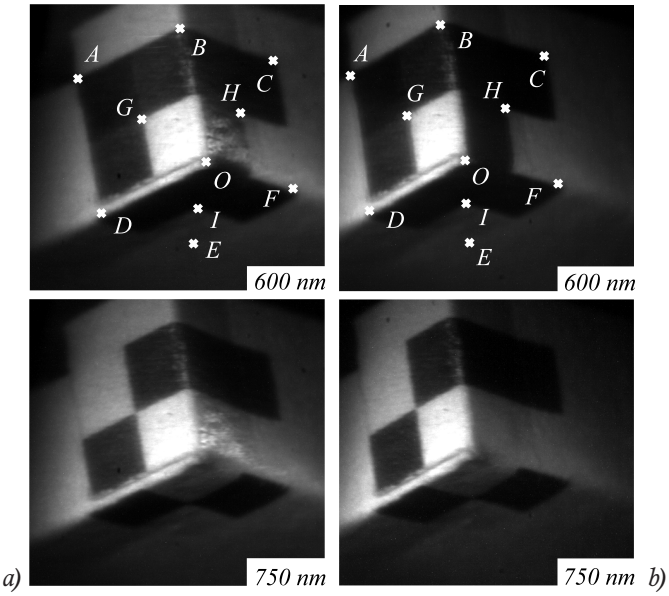

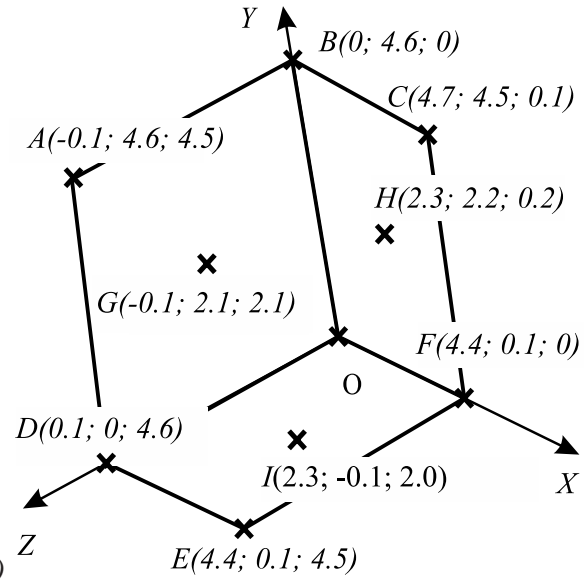

Fig. 3. Recorded spectral images (a) and 3D point coordinates of the object surface restored thereon (b)

Discussion

The developed spectral stereoscopic imaging system allows us to select and register two light beams reflecting the observed object in two different perspectives and at an optional wavelength wherein the beams have mutually orthogonal polarization. If the object doesn't have any polarization properties and, for this reason, the image doesn't depend on polarization, it is possible to restore the 3D object image by this pair of images using computer vision methods. The study has shown that the resulting pair of images has sufficiently high quality and quite substantial identity. If the images in two polarizations have notable differences, this may affect the quality of restored images of the object surface. However, even in this case, a set of key points allows us to reconstruct a surface "frame" that is sufficient to determine the total shape of a segment of the observed object.

As seen, the installed system shall actually function as a spectral polarimeter for heavily polarizing objects, i.e. it allows us to determine polarization characteristics for various object points at random wavelengths. In addition, the object shape can be also reconstructed if the object has well-defined geometric characteristics (angles, edges, etc.) or spectral intensity features (shaded recesses or strongly diverging ribs, for example, scratches). In many cases, when there is prior information on object properties (a polyhedron, a blister, etc) the exact form of the object surface may be reconstructed by its key points. In this case, it is possible to simultaneously determine spatial, spectral, and polarization characteristics.

It should also be noted that some technical problems have been solved upon making the stereoscopic spectrometer [18]. Since its layout is based on the use of two acousto-optical cells, either of which is a complex active device, it is necessary to provide, first, their identity in manufacturing and assembling; second, their synchronization, and third, their preliminary calibration to be performed. The divergence of channel tuning wavelengths, when delivering the frequency from a single high-frequency generator because of difference in their tuning characteristics, would not allow us to obtain high-contrast images simultaneously in two channels and, accordingly, to achieve the stereo effect.

Conclusion

The optical system that generates stereoscopic images of micro-objects in separate narrowband spectral channels with high spectral (about 2 nm) and spatial (500 x 500 elements) resolution was first developed. The system also allows you to analyze the state of the object radiation polarization. The system has small dimensions and no moving elements and, therefore, it can be used in applications where these properties are the most important and durable, for example, in express measurements *in situ*.

Acknowledgements

The work was funded by RFBR, Project No. 16-08-01278 and 16-07-00393.

References

1. Chang IC. Hyperspectral imaging: techniques for spectral detection and classification. Springer; 2003.

2. Boas D, Pitris C, Ramanujam N. Handbook of biomedical optics. CRC Press; 2011.

3. Yoon S, Thai C. Stereo spectral imaging system for plant health characterization. Proc ASABE Annual Int Meeting 2009 Reno, Nevada, June 21 - June 24: 096583. DOI: 10.13031/2013.27167.

4. Pozhar V, Machihin A. AOTF-based 3D spectral imaging system. AIP Conf Proc 2012; 1433(1): 65-67. DOI: 10.1063/1.3703140.

5. Machikhin AS, Pozhar VE. Stereoscopic 3-dimensional spectral imaging systems based on a single acousto-optical tunable filter. J Phys: Conf Ser 2015; 661: 012041.

6. Begunov BN, Zakaznov NP, Kiryushin SI, Kuzichev VI. Optical instrumentation. Theory and design. Moscow: "MIR" Publishers; 1988.

7. Goutzulis A, Rape D. Design and fabrication of acousto-optic devices. New York: Marcel Dekker, Inc.; 1994.

8. Pozhar VE, Pustovoit VI. Acousto-optical spectral technologies. Bulletin of Russian Academy of Sciences. Physics 2015; 79(10): 1221-1226. DOI: 10.3103/S1062873815100202.

9. Chang IC. Analysis of non-collinear acousto-optic filters. Electron Lett 1975; 11(25). P. 617-618. DOI: 10.1049/el:19750470.

10. Machikhin AS, Pozhar VE. Image transformation caused by wide-angle acousto-optic interaction. Quantum Electronics 2010; 40(9): 837-841.

11. Mazur MM. Physical and technological basics of acousto-optic devices [in Russian]. Doctoral thesis. Moscow: "NTC UP RAN" Publisher; 2007.

12. Polikarpova NV, Voloshinov VB, Reznikov AM. Development of acousto-optic edvices based on transformation of acoustic waves. Phys Wave Phen 2015; 23(1): 52-57.

13. Voloshinov VB, Bogomolov DV. Effect of the parameters of a wide-aperture acousto-optic filter on the image processing quality. Quantum Electronics 2006; 36(5): 457-463.

14. Hartley RI, Zisserman A. Multiple View Geometry. Cambridge: Cambridge University Press; 2000.

15. Forsyth DA, Ponce J. Computer Vision: a Modern Approach.

Upper Saddle River: Prentice-Hall; 2012. ISBN: 978-0-13-608592-8.

16. Gorevoy AV, Machikhin AS. Method to improve accuracy of the geometrical parameters measurement in stereoscopic AOTF-based spectral imagers. Journal of Physics: Conference Series 2015; 584(1): 012004.

17. Gruzman IS, Kirichuk VS, Kosykh VP, Peretyagin GI, Spector AA. Digital image processing in information systems [in Russian]. Novosibirsk: "NGTU" Publisher; 2000.

18. Machikhin AS, Pozhar VE. Obtaining spectral stereo images with electronic spectral tuning and polarization separation. Tech Phys Lett 2014; 40(9): 803-806. DOI: 10.1134/S1063785014090247.